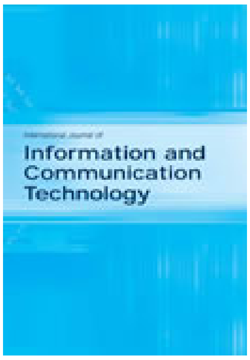

International Journal of Information and Communication Technology

ISSN online: 1741-8070 - ISSN print: 1466-6642
https://www.inderscience.com/ijict

Monitoring and early warning of regional subsidence of transmission lines based on time series algorithm

Lin Guo, Ge Liu, Shaolei Chen, Xiaolei Zhang, Xu Lu

Article History:

Received:	23 July 2024
Last revised:	26 September 2024
Accepted:	26 September 2024
Published online:	22 January 2025

Monitoring and early warning of regional subsidence of transmission lines based on time series algorithm

Lin Guo*, Ge Liu, Shaolei Chen and Xiaolei Zhang

State Grid Sichuan Electric Power Company,
Chengdu, China
Email: 11348585@qq.com
Email: 19641218@163.net
Email: chenslzju@163.com
Email: mumulei0411@126.com
*Corresponding author

Xu Lu

State Grid Sichuan Neijiang Power Supply Company,
Neijiang, China
Email: 119796502@qq.com

Abstract: This paper models the monitoring and early warning task of surface subsidence in the high-voltage line tower area, this study uses PS-InSAR technology to preprocess the clipped satellite remote sensing images to obtain surface subsidence data, the predicted values and deformation curves are basically coincident, and the trend of change is basically consistent. The absolute error of settlement prediction is less than 1%, indicating high prediction accuracy. From the experiment, it can be seen that this improvement effectively improves the system accuracy and reduces prediction errors. From the experimental results, it can be seen that the monitoring and early warning model of regional subsidence of transmission line based on the time series algorithm proposed in this paper has a certain effect, and can meet the needs of monitoring and early warning of regional subsidence of transmission lines.

Keywords: time series; transmission lines; regional subsidence; monitoring; early warning.

Reference to this paper should be made as follows: Guo, L., Liu, G., Chen, S., Zhang, X. and Lu, X. (2025) 'Monitoring and early warning of regional subsidence of transmission lines based on time series algorithm', *Int. J. Information and Communication Technology*, Vol. 26, No. 2, pp.1–22.

Biographical notes: Lin Guo obtained her Master's in Information and Communication Engineering from Chengdu University of Technology and currently works at State Grid Electric Power Company Information and Telecommunication Company, with a research focus on power communication technology.

Ge Liu obtained his PhD in Physics Electronics from University of Electronic Science and Technology of China, currently works at Electric Power Dispatching and Control Center of State Grid Sichuan Electric Power Company as a Professor Senior Engineer. He is dedicating the technology research, planning, design, construction, and maintenance of the company's communication network and selected as an expert Judge of the Ministry of Science and Technology of the People's Republic of China.

Shaolei Chen obtained his PhD in Information and Communication Engineering from Zhejiang University, and currently works at Electric Power Dispatching and Control Center of State Grid Sichuan Electric Power Company, with a research focus on power system and communication technology.

Xiaolei Zhang obtained her Master's and PhD of Engineering in Information and Communication Engineering from Gongju University (National University of Korea) and currently works at State Grid Sichuan Leshan Power Supply Company, with a research focus on power communication technology.

Xu Lu obtained a master's degree in Project Management from University of Shanghai for Science and Technology, and currently works at State Grid Sichuan Neijiang Power Supply Company, with a research focus on Relay Protection of Power System and Smart Grid Dispatch.

1 Introduction

As an indispensable part of transmission lines, transmission towers play a key role in supporting conductor and ground wires. Therefore, the improvement of power supply reliability of power transmission and distribution lines in power grids largely depends on the safe and stable operation of transmission towers. However, with the increasing scale of power grids, higher voltage levels of transmission lines, longer transmission distances, and greater transmission capacities, the operating conditions and environment of power systems have also become more complex. Due to the inevitable frequent operation of transmission towers in special areas such as mining areas, river beaches, and hillsides, it is very easy to cause faults such as the sinking of the tower foundation, the inclination of the tower body, the deformation of the tower material, the disconnection of the conductor, and even the collapse of the tower. Moreover, the tower fault is a typical 'invisible fault'. During the normal manual inspection of the transmission line, it is often not found in time. When the tower fault is found, the transmission line is already in a relatively dangerous state, seriously threatening the reliable operation of the line (Wu et al., 2022).

The uneven subsidence of ground difference will cause the transmission tower to tilt laterally, resulting in the structure to bear uneven tension, and in severe cases, the fittings, insulators, conductors, transmission lines and transmission towers will be damaged to varying degrees, thereby affecting the normal operation of the power system. Although large foundation subsidence is a small probability event, once this happens, it will not only destroy the line, but also interrupt the entire transmission system, and even may cause the transmission towers to overturn, resulting in the paralysis of the entire power system (Xu et al., 2022).

The monitoring equipment installed on the tower can record the status and operation parameters of the equipment in real-time through the real-time online monitoring system of the transmission line. The important measure of condition maintenance and realisation of condition monitoring is online monitoring system, and the success of online monitoring technology largely determines the possibility of realisation of condition maintenance. Moreover, unattended remote monitoring can provide auxiliary judgment and guidance for line inspectors to carry out line condition maintenance, provide important technical means for improving the level of production and operation, realise real-time management of line status, and escort the normal operation of smart grid (Yang et al., 2020). In addition, online monitoring of tower tilt, environmental factors and other related parameters by modern sensing means can sense the operation information of the line in real-time and warn of possible accidents, which have great significance for maintaining the safety of the line.

The purpose of this paper is to study the monitoring and early warning of regional subsidence of transmission lines by building a model based on time series algorithm. this study uses PS-InSAR technology to preprocess the clipped satellite remote sensing images to obtain surface subsidence data, it can be seen that the monitoring and early warning model of regional subsidence of transmission line based on the time series algorithm proposed in this paper has a certain effect, and can meet the needs of monitoring and early warning of regional subsidence of transmission lines.

2 Related work

The research on mining subsidence discipline was conducted earlier in foreign countries, and the 20th century was a century of rapid development and gradual maturity in this discipline. On the basis of actual investigation, Liu et al. (2021) simplified the rock and soil in contact with cavities as an ideal linear elastic medium and studied the settlement and failure mechanism of rock and soil under elastic limit conditions. Chen et al. (2023) use the rock layer above the goaf as a cantilever beam and derives the theory that surface strain is inversely proportional to curvature radius. Rodríguez-Arana et al. (2023) applied mathematical plasticity theory to propose the famous argument that the sinking profile equation takes the form of an exponential function and that horizontal movement is directly proportional to surface tilt. Godse and Bhat (2020) proposed the theory of stochastic media, which treats rock movement as a stochastic process. Leber et al. (2020) proposed the panel principle using elastic theory, combining continuum mechanics with the influence function method, laying the foundation for the current boundary element method. Li et al. (2024) summarised and summarised the prediction methods for coal mining subsidence, proposed the influence function of horizontal movement, and developed the circular integral grid method to calculate surface movement.

Huang (2020) used probability integration method to predict surface subsidence caused by insufficient mining in the working face under a certain mining industrial square. Corresponding building protection measures have been proposed. In the past, when studying issues such as surface movement and deformation, for the sake of convenience, people often oversimplified the overlying rock layers, either as a single loose medium or as a pure elastic medium. Overly idealised models often differ greatly from reality, especially when there are thick loose layers, using the single medium theory is not only difficult in theory, but also deviates greatly in practice.

Accidents such as tilting, sinking, cracking, deformation, and breakage of transmission line towers are mainly caused by the following two factors: geological instability around the tower foundation and imbalance of tension on both sides of the tower. To a large extent, the generation and development process of transmission tower faults is very complex, including many random factors, which cannot be analysed based on relevant basic theories. Effective measurement methods and online monitoring technology can only be relied on to timely discover the collapse and deformation characteristics of goaf, timely grasp and predict early changes such as tower ground collapse and ground settlement, and then take corresponding preventive measures. The application of online monitoring and fault diagnosis methods for transmission lines mainly relies on monitoring the deformation degree of iron towers using angle sensors and comprehensive analysis and judgment of the overall deformation degree of iron towers using satellite remote sensing technology (Ansari et al., 2021). These methods can play a good substitute role for relying solely on traditional inspections to detect faults in the past. If we want to grasp the relationship between the actual settlement and inclination of the iron tower and the force on the iron tower, a lot of analysis and experimental verification work needs to be done, so it cannot guide the safe operation and condition maintenance of the iron tower. The stress monitoring technology for transmission towers is to directly and effectively monitor the stress and strain signals of the members, and consider the structural characteristics of the tower, ultimately reflecting the degree and location of local structural damage to the tower. The stress borne by transmission tower members represents a force generated by themselves when subjected to external loads, which varies with the magnitude of external loads. At the same time, its magnitude can be used to characterise the overall safe stress state of the tower (Brito Palma, 2024). At present, there are three widely used methods for monitoring stress and strain: first, electrical measurement method; For example, the electrical measurement method based on resistance strain gauges has high sensitivity and belongs to contact measurement. The signal conditioning circuit is simple, and the measurement accuracy is also relatively high. It is suitable for most occasions and has a wide range of applications (Liu et al., 2020). Secondly, visual measurement method can follow the movement of the target, and its measurement accuracy is closely related to the performance of the camera. It is mainly used in non-contact measurement situations (Abasi et al., 2022). Thirdly, optical measurement methods; For example, stress measurement based on fibre Bragg gratings has developed rapidly, but there are still issues such as temperature and strain cross sensitivity, and demodulation of fibre optic sensing signals that need to be further addressed (Wu et al., 2021). Currently, only by proposing a method that combines stress analysis of transmission towers with monitoring technology can the safe operation status of transmission towers be continuously monitored and evaluated, making monitoring data an important basis for guiding condition maintenance. Therefore, the method of stress monitoring and shape recognition system for transmission towers based on resistance strain gauges will achieve real-time monitoring of stress information of key member units under settlement, tilting, and lateral sliding conditions of transmission towers. Based on the position and stress value of key member units, the current working condition and settlement displacement value of the tower will be restored and real-time warning will be provided, providing a basis for the evaluation and maintenance of the tower’s condition. In addition, the operational monitoring data of this system can also be used as a stress database for key member units, promoting in-depth research on stress monitoring and failure mechanisms of key member units in iron towers, thereby providing reference for tower deformation correction,

correction, and monitoring, and further supplementing the completed research results (Kozyreva et al., 2022).

Time series displacement prediction models have become a hot research topic in recent years. As a mature observation method in long-term displacement monitoring, InSAR has been proposed by some scholars to combine InSAR with prediction models, which can better predict displacement in time series. Chen (2020) combines SBAS InSAR technology with grey support vector machine (GM-SVR) model to monitor and predict the deformation of residential areas caused by mining in mining areas, providing a reference method for disaster warning in subsidence areas. Chen et al. (2024) compared the surface subsidence monitoring data obtained by D-InSAR technology with GM and its improved three models for subsidence prediction. After comparison, it was found that the optimised BGM (1,1) model and WGM (1,1) model can effectively reduce the errors generated by the classical GM model. Khayrullaev (2023) combines InSAR technology with a time model to predict dynamic 3D mining displacement. Firstly, the Weibull model and Kalman filter are used to predict the line of sight (LOS) mining displacement of the dynamic radar point by point. Then, combined with common prior information related to mining deformation, the 3D displacement is calculated from the predicted LOS displacement. Chehri et al. (2021) used the settlement values obtained by D-InSAR technology as training samples and established a settlement prediction system in conjunction with SVM prediction models, which can achieve the integration of deformation monitoring and prediction. Lazzaretti et al. (2020) proposed a method for learning surface subsidence features based on multi main image coherent target small baseline interferometry (MCTSB InSAR) and LSTM model. The model parameters were adjusted using grid search to obtain the optimal model parameters for predicting surface subsidence.

3 Research methods

3.1 Data preprocessing

This article focuses on the initial data collection of settlement data in the area of high-voltage transmission towers. The research area has the characteristics of wide coverage, difficult data collection, complex geographical environment, and difficult maintenance of monitoring facilities. The monitoring work is difficult, and traditional surface settlement monitoring techniques cannot meet the requirements. Therefore, this article collects satellite remote sensing images as basic data, establishes an environmental database in complex environments, continuously supplements database data through intelligent learning, compares imported data with database data, and combines multi-dimensional data fusion technology to improve data preprocessing efficiency.

The initial data collection of the subsidence data of the high-voltage line tower area shows that the research area has the characteristics of wide coverage, difficult data collection, complex geographical environment, and difficult maintenance of monitoring facilities. Moreover, the monitoring work is difficult, and the traditional surface subsidence monitoring technology cannot meet it. Therefore, this paper collects satellite remote sensing images from Sentinel-1A as basic data. Meanwhile, in this study, PS-InSAR technology is used to preprocess the clipped satellite remote sensing images, SARProz software is used as the experimental platform, and Matlab2022 is used as the operation basis to obtain surface subsidence data. The preprocessing process of meteorological and environmental factor data in this paper is shown in Figure 1.

Figure 1 Flow chart of pretreatment of meteorological and environmental factors (see online version for colours)

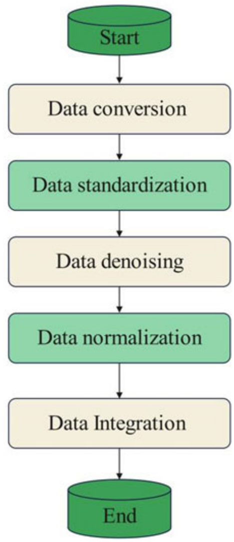

The range of meteorological and environmental factors is different, so the data are normalised to speed up the convergence speed of the model. This paper uses the z-score method to perform data normalisation processing. The formula is as follows:

$$Z = \frac{x - \mu}{\sigma} \tag{1}$$

Among them, x represents the original data, μ represents the mean value of the original data, and σ represents the standard deviation of the original data. Through data normalisation processing, different features can be in the same scale range, so as to avoid the problem that different feature scales have different effects on model training.

3.2 *Time series forecasting*

In this study, the relationship between the meteorological research site and various PS monitoring sites is established, and the subsidence monitoring results of high-voltage line towers are obtained. By calculating the straight-line distance between each PS monitoring point and the meteorological research point, the nearest meteorological research point is taken, so as to confirm the meteorological and environmental factors data of each PS monitoring point. We assume that there are two sets P and W, where set P contains n monitoring points and set W contains m meteorological study points, and they are represented as $P = \{(x_1, y_1), (x_2, y_2), \ldots, (x_n, y_n)\}$ and $W = \{(a_1, b_1), (a_2, b_2), \ldots, (a_m, b_m)\}$, respectively. In order to determine the data matching between P and W, this paper chooses the minimum distance as the matching distance by calculating the distance between each monitoring point and each study point.

For each monitoring point (i, i) in P, the distance between it and each study point (k, k) in W is calculated:

$$dis(i, k) = \sqrt{(x_i - a_k)^2 + (y_i - b_k)^2} \tag{2}$$

Then, the smallest value $min(dis(i, k))$ is selected from these distances, and the data match between P and W is determined by comparing the smallest distance between all monitored and studied sites. The minimum of all distances is selected as the matching distance between the two points by calculating the distances between all monitoring points in P and all study points in W. Then, the (a_k, b_k) matched to the minimum distance is given to (x_i, y_i) as its meteorological point data, and it can be determined that there is a data matching relationship between (a_k, b_k) and (x_i, y_i), otherwise there is no matching relationship between them.

3.3 Foundation model

The main components of transformer include encoder and decoder, and its network structure is shown in Figure 2.

Figure 2 Transformer network structure (see online version for colours)

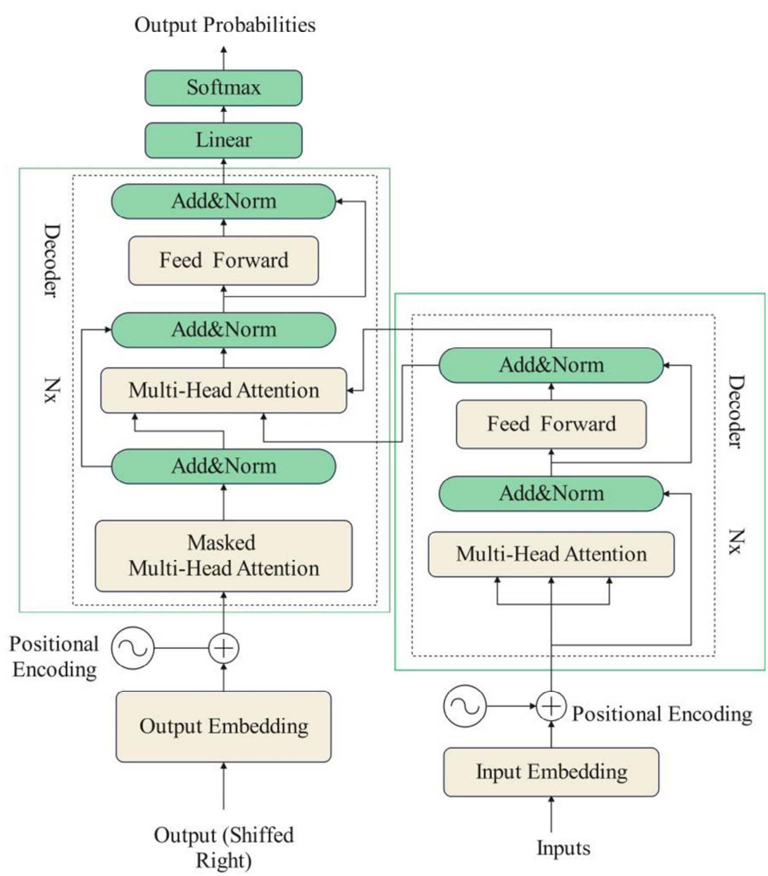

The encoder is a stack of n layers with the same structure, and the residual connection and layer normalisation are used in the middle of each sublayer to avoid the problem of gradient disappearance. The output for each sublayer is:

$$LayerNorm\left(x + Sublayer(x)\right) \tag{3}$$

Among them, x is the input sequence, *LayerNorm* represents the normalised layer, and $Sublayer(x)$ represents the sub-layer itself (multi-head self-attention or feed-forward neural network). The structure of the decoder side is also a stack of n layers of the same structure, and the overall structure is similar to that of the encoder. The difference is that a third sublayer is added here. The result of self-attention is used as query, and the output of the encoder is used as Key and Value for cross-attention. In addition, a mask is added to the bulls' attention part here, so that all positions after the current predicted position are masked off to retain the autoregressive characteristics of the model.

Because transformer is based on a fully connected network structure, it lacks position information in convolution operations. To solve this problem, transformer uses position coding. Position coding is to embed the position information of each element in the sequence into the vector, so that the model can distinguish the distance relationship between elements. The sine and cosine functions are used, and the calculation formula is as follows:

$$PE_{(pos,2i)} = \sin\left(pos / 10000^{\frac{2i}{d}}\right) \tag{4}$$

$$PE_{(pos,2i+1)} = \cos\left(pos / 10000^{\frac{2i}{d}}\right) \tag{5}$$

Among them, pos represents the position, i represents the dimension in the position coding, and d represents the dimension of the embedded vector. The advantage of position coding is that it can effectively capture the distance relationship between elements, so as to help the model understand the order information in the sequence. Moreover, the calculation amount of position coding is small, and it will not increase too many model parameters, so it will not affect the calculation efficiency of the model too much. The self-attention mechanism is a core component of Transformer, which can find relevant information in the input sequence and perform weighted summarisation at different positions.

The attention weight of each element is determined by performing a SoftMax operation on the attention score and converting it into a probability distribution. The calculation formula is:

$$Attention(Q, K, V) = soft\max\left(\frac{Qk^T}{\sqrt{d_k}}\right)^V \tag{6}$$

Among them, Q, K, and V represent the query vector (query), key vector (key), and value vector (value) respectively, k^T is a scaling factor, and d_k represents the vector dimension. The model proposes a multi-head attention mechanism, which uses a group of mapping matrices $W_i^Q \in R^{d_{model} \times d_q}$ to map key vectors, query vectors and value vectors respectively. Each i corresponds to one of the heads:

$$head_i = Attention\left(QW_i^Q, KW_i^K, VW_i^V\right) \tag{7}$$

Among them, *Attention*( ) is the scaling dot product attention mechanism described above. All the heads are then outputted and then mapped to the original dimensions d_{model} using a mapping matrix.

$$MultiHead(Q, K, V) = Concat\left(head_1, ..., head_h\right)W^0 \tag{8}$$

Due to the excellent performance of the transformer model in time series analysis modelling and prediction, this paper uses it to model the dataset in this paper to realise the prediction of the subsidence value of the high-voltage line tower area, and uses it as a benchmark model to compare and evaluate with other models.

Based on the idea of moving average, smooth period items and highlight trend items are:

$$X_t = AvgPool\left(Padding(X)\right) \tag{9}$$

$$X_s = X - X_t \tag{10}$$

Among them, X is the hidden variable to be decomposed, X_t and X_s are the trend term and the period term respectively. In the encoder part, autoformer gradually eliminates the trend term (this part will be accumulated in the decoder) to obtain the periodic term $S_{en}^{l,1}$ and $S_{en}^{l,2}$. The information aggregation process can be expressed as:

$$S_{en}^{l,1} = SeriesDecomp\left(AutoCorrelation\left(X_{en}^{l-1}\right) + X_{en}^{l-1}\right) \tag{11}$$

$$S_{en}^{l,2} = SeriesDecomp\left(FeedForward\left(S_{en}^{l,1}\right) + \left(S_{en}^{l,1}\right)\right) \tag{12}$$

$$S_{en}^{l,1}, T_{de}^{l,1} = SeriesDecomp\left(AutoCorrelation\left(X_{de}^{l-1}\right) + X_{de}^{l-1}\right) \tag{13}$$

$$S_{en}^{l,2}, T_{de}^{l,2} = SeriesDecomp\left(AutoCorrelation\left(S_{de}^{l,1}, X_{en}^{N}\right) + S_{de}^{l,1}\right) \tag{14}$$

$$S_{en}^{l,3}, T_{de}^{l,3} = SeriesDecomp\left(FeedForward\left(S_{de}^{l,2}\right) + S_{de}^{l,2}\right) \tag{15}$$

$$T_{de}^{l} = T_{de}^{l-1} + W_{l,1} * T_{de}^{l,1} + W_{l,2} * T_{de}^{l,2} + W_{l,3} * T_{de}^{l,3} \tag{16}$$

For a real discrete-time process $\{X_t\}$, autoformer calculates its autocorrelation coefficients $R_{xx}(\tau)$ based on the stochastic process theory:

$$R_{xx}(\tau) = \lim_{L \to \infty} \frac{1}{L} \sum_{t=0}^{L-1} x_t x_{t-\tau} \tag{17}$$

Among them, the autocorrelation coefficient $R_{xx}(\tau)$ represents the similarity between the sequence $\{X_t\}$ and its τ delay $\{X_{t-\tau}\}$. Autoformer regards this delay similarity as an un-normalised period estimation confidence level, that is, the confidence level of a period length of τ is $R(\tau)$.

Autoformer realises sequence-level connection by aggregating similar sub-sequence information. According to the estimated cycle length, the information is aligned by using ROLL function operation, and then the information is aggregated in the form of query, key, and value, so that the seamless replacement of the self-attention mechanism is realised.

$$\tau_1, ..., \tau_k = \arg Topk\left(R_Q, k(\tau)\right) \tau \in \{1, ..., L\} \tag{18}$$

$$\widehat{R}_Q, k\left(\tau_1\right), ..., \widehat{R}_Q, k\left(\tau_k\right) = SoftMax\left(R_Q, k\left(\tau_1\right), ..., R_Q, k\left(\tau_k\right)\right) \tag{19}$$

$$AutoCorrelation(Q, K, V) = \sum_{i=1}^{k} Roll\left(V, \tau_k\right) \widehat{R}_Q, k\left(\tau_k\right) \tag{20}$$

Due to the excellent performance of autoformer model in long-term time series analysis modelling and prediction, this study uses it to model the dataset in this paper to realise the prediction of the subsidence value of high-voltage line towers, and uses it as a benchmark model to compare and evaluate with other models.

4 Model and experimental analysis

4.1 Model construction

This article predicts the settlement values of various PS monitoring points in the research area, calculates the surface settlement rate, and establishes a complete settlement warning model for high-voltage transmission tower areas based on the cumulative settlement values and settlement rates. This model can provide risk level warnings for the predicted cumulative settlement values of each PS monitoring point. In order to reduce the systematic error caused by severe weather on the model, this paper adopts a method of comprehensive data induction and processing for different monitoring points. When the data of one point is abnormal due to severe weather, it is compared with the data of other nearby points, and combined with visualisation data technology for comprehensive judgment, to minimise the impact of severe weather on prediction accuracy

Figure 3 Schematic diagram of CORS working process (see online version for colours)

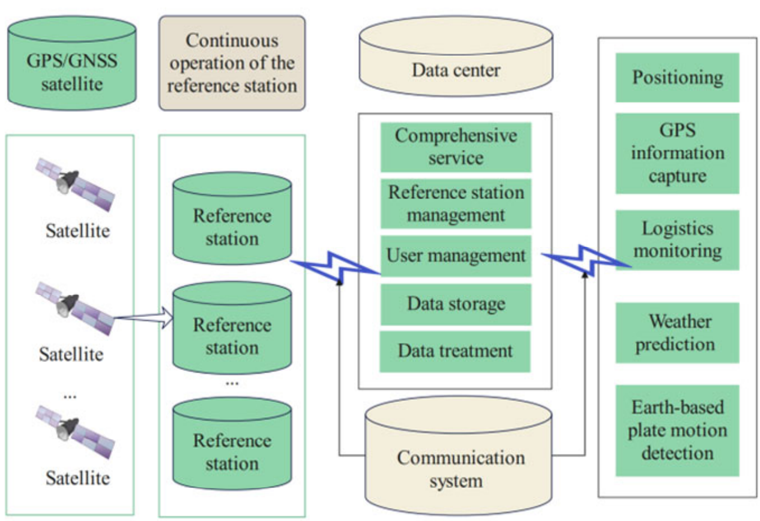

Continuously operating reference system (CORS) builds a local area network system in a local area composed of several continuously operating reference stations to provide users with GPS navigation and positioning related services. It is composed of several continuously running reference stations, data communication link layer, data centre and user terminal. The schematic diagram of the CORS working process is shown in Figure 3.

Figure 4 CORS hardware system and data flow (see online version for colours)

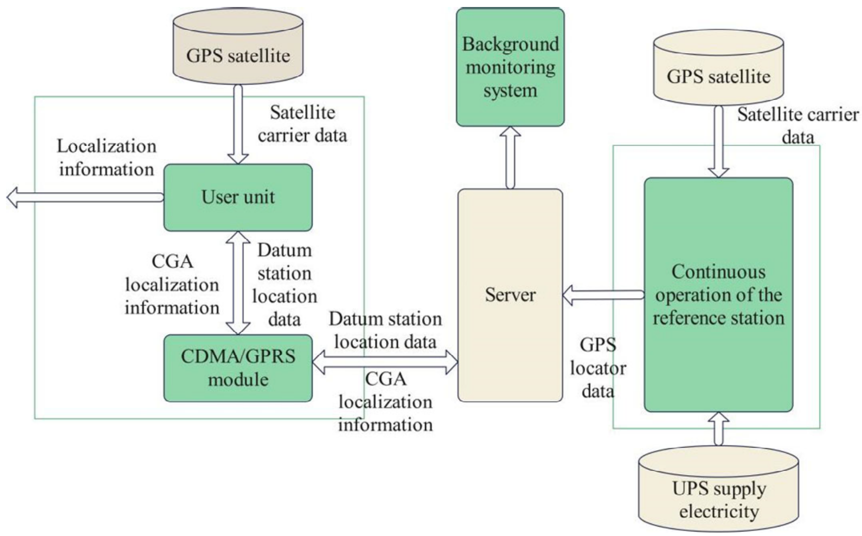

Figure 5 CORS structure diagram (see online version for colours)

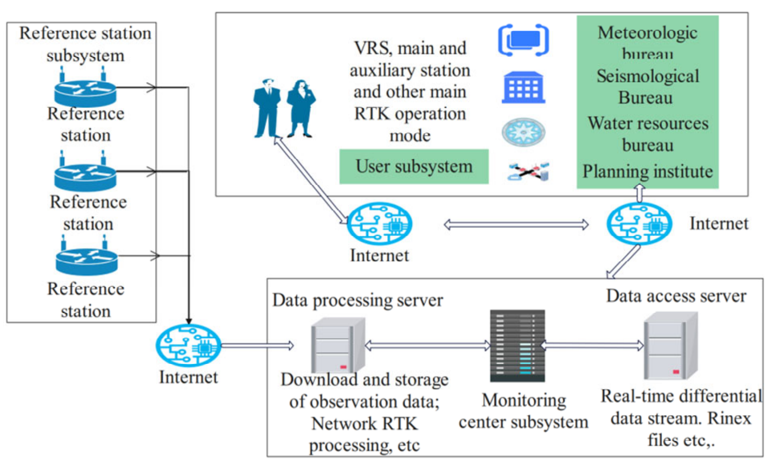

The working principle of CORS is: It establishes one or more continuous GPS reference stations in a region or a country, and forms an organic network with the monitoring centre to automatically send different GPS original data and RTK correction information to various users. At this time, users only need a GPS receiver to achieve high-precision, real-time navigation and positioning. The data centre collects the data processed by the network software from the reference station and shares it in a wide area to meet the needs of different users in the society. The CORS hardware system and data flow are shown in Figure 4, which has the characteristics of all-weather, automatic, real-time navigation and positioning.

The CORS system is composed of a monitoring centre subsystem, a reference station subsystem, and a user subsystem, as shown in Figure 5.

1 The monitoring centre subsystem is the brain part of CORS, consisting of two parts: the user management centre and the system data centre. Not only responsible for analysing, processing, calculating, and storing GPS satellite positioning raw data, but also building a virtual reference station system model, generating differential correction data information, and transmitting, recording, managing, and maintaining it. Effectively manage user information and provide corresponding positioning services to users. So the monitoring centree subsystem is a guarantee for the safe, reliable, and continuous operation of the CORS system.

2 The reference station subsystem is composed of a GPS receiver, GPS antenna, power supply, network equipment system, and lightning protection system. Responsible for GPS satellite positioning tracking, collection, and storage, transmitting data to the system data centre of the monitoring centre subsystem, it is the GPS satellite data receiving functional unit of the CORS system.

3 The user subsystem consists of a GPS receiver, GPS antenna, and communication submodule, and is the end user of the CORS system. The end user receives the RTK differential correction data shared by the monitoring centre subsystem through the communication module, while the GPS antenna receives the original satellite data, which is then analysed and processed by the GPS receiver. After differential processing, the end user obtains high-precision positioning information.

Schematic diagram of the system as shown in Figure 6. This article is mainly responsible for transmitting the correction data of the GPS system to the monitoring mobile station. When the deviation exceeds the warning value, it will alarm in a timely manner to eliminate power accidents in the bud.

Figure 6 Schematic diagram of the system (see online version for colours)

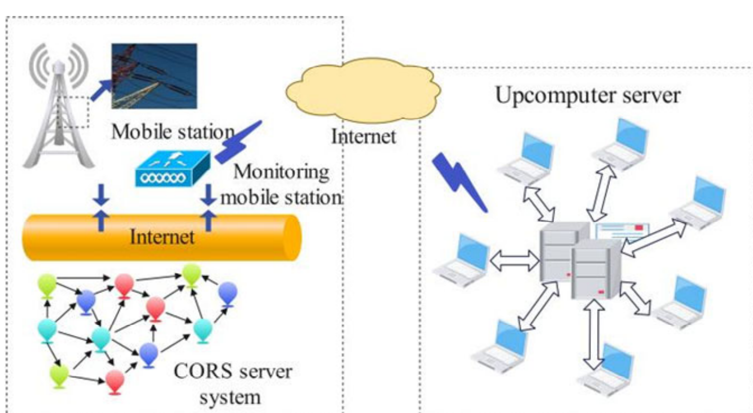

Figure 7 Basic flow chart of SBAS-In SAR (see online version for colours)

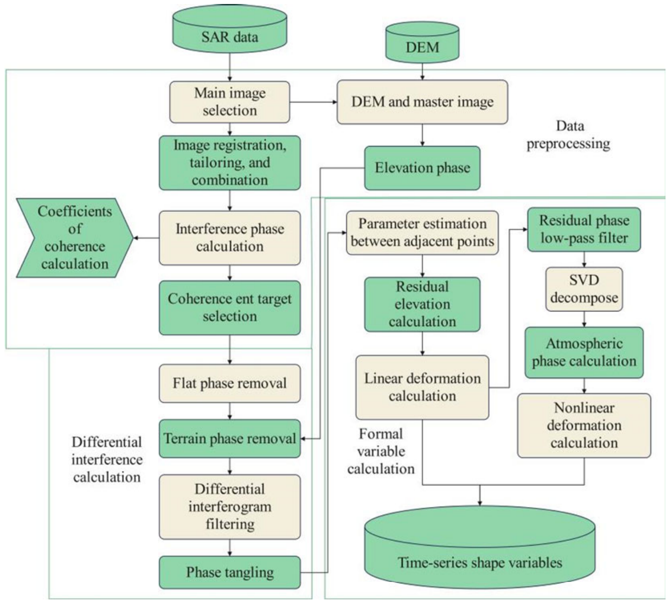

In reality, the ground objects collected by the satellite in the second return visit usually have a certain degree of deformation. Therefore, the radar interferometric phase includes not only the flat ground phase and terrain phase caused by reference ellipsoid and elevation change, but also the noise phase caused by other factors, and the deformation phase caused by surface deformation. The basic method of In SAR to monitor the surface deformation information is to remove the remaining phase, so as to obtain the deformation phase caused by the surface deformation. Small baseline subset in SAR (SBAS-In SAR) divides all SAR images that meet the conditions into several small sets by setting different spatio-temporal baselines, and simply and efficiently synthesises all available small baseline interference pairs. Then, based on the minimum norm criterion of the deformation rate, it uses the singular value decomposition (SVD) method to obtain the deformation rate of the ground target point, as shown in Figure 7.

4.2 Experiments

The development language of the host computer server software of the transmission tower attitude monitoring and analysis system is Visual Basic. NET, the development environment is Microsoft Visual Studio 202022, and the database used is Microsoft Office Access 2022. The server software consists of five parts: system setting, user management, network service, equipment management and data centre. The overall framework of the host computer server software is shown in Figure 8.

The main operation interface of the host computer server is shown in Figure 9. The main interface displays the three-dimensional model for monitoring the attitude of the transmission tower of the mobile station and other parameters related to the monitoring mobile station. Moreover, the early warning value is set in the system settings. When the monitoring value of the monitoring mobile station exceeds the early warning value, it will alarm and prompt the staff to solve emergencies. In addition, the setup functions of the system include initial setup, start service/pause service, and exit the system. When users first use the software, they need to configure initial values, including longitude, latitude and altitude, X-direction tilt angle, Y-direction tilt angle and Z-direction tilt angle.

Figure 8 Function of host computer server software system (see online version for colours)

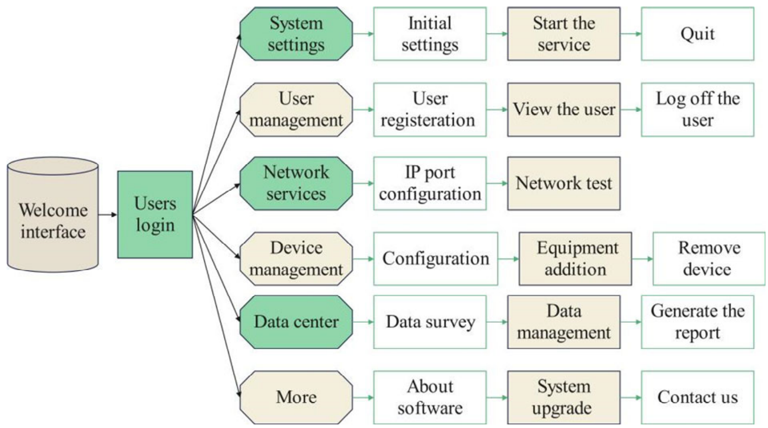

Figure 9 The main interface of the host computer server (see online version for colours)

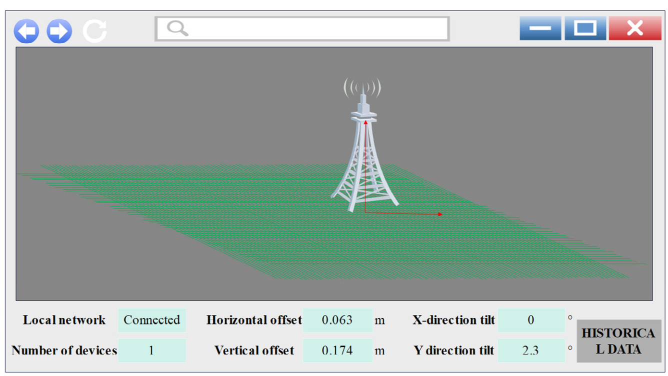

Combined with the existing research, it can be seen that LSTM has a higher accuracy in predicting wave displacement, while Elman has a better effect in predicting trend displacement.

After that, this paper proposes a neural network prediction model Elman-LSTM, which combines LSTM and Elman. First, the cumulative displacement value of the study area is calculated by SBAS. Taking a transmission line area as an example, 10 sampling points are selected, and 82 periods of data from each sampling point are used for model training and prediction. Then, the total cumulative displacement obtained by SBAS is decomposed into wave displacement and trend term displacement by time series decomposition principle, and the wave displacement is predicted by LSTM model, and the trend term displacement is predicted by Elman model. Finally, the final cumulative total displacement is obtained by accumulating the displacements predicted by the two models.

4.3 Results

The displacement prediction results of the Elman-LSTM model for point N are shown in Figure 10.

Figure 10 Displacement prediction result diagram (N) of Elman-LSTM, (a) prediction of the trend-term displacement at point A (b) prediction of the fluctuation term displacement at point A (c) cumulative displacement prediction at point A (d) the cumulative displacement prediction interval at point A (see online version for colours)

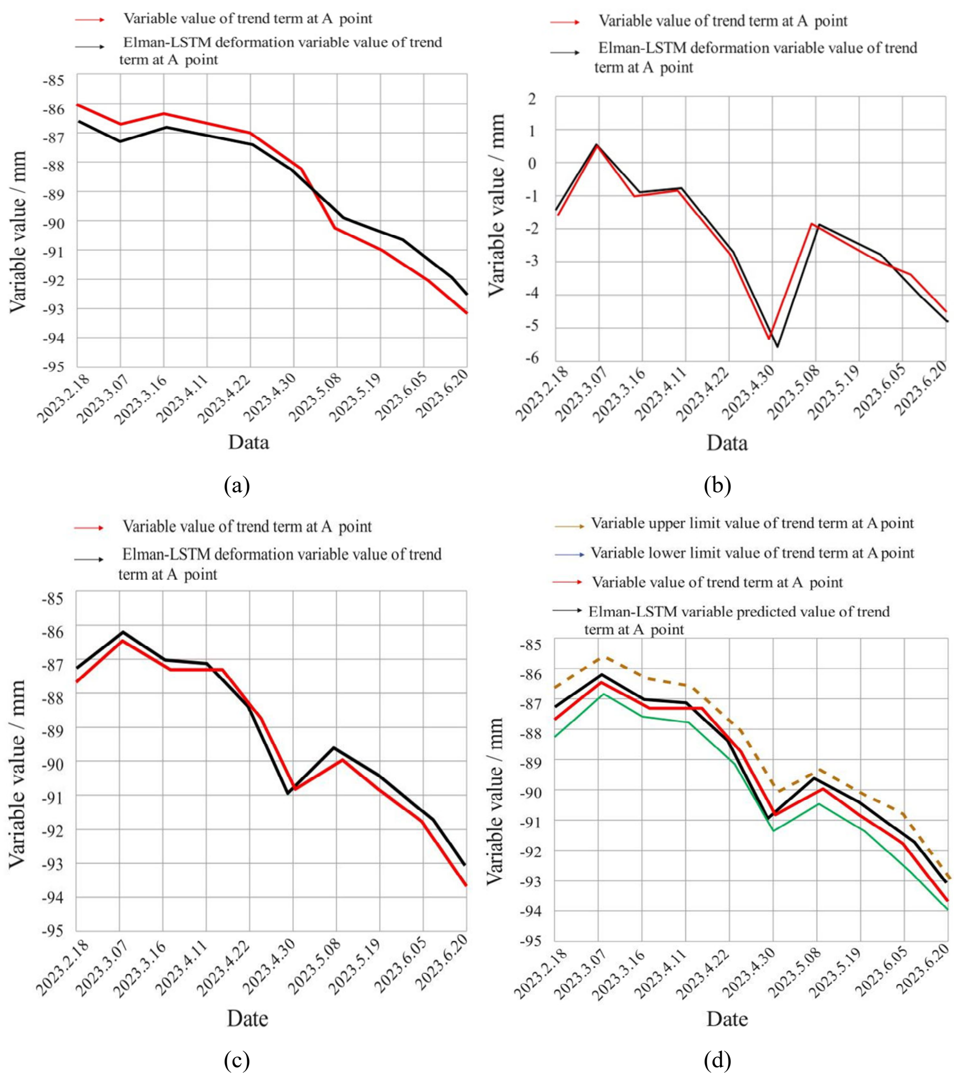

In order to further analyse the data, the data in Figure 10(c) are counted, and the corresponding absolute errors and relative errors are calculated. The specific values are shown in Table 1.

The displacement prediction results of Elman-LSTM model for point A are shown in Figure 11.

Figure 11 Displacement prediction result diagram (B) of Elman-LSTM, (a) prediction of the trend-term displacement at point B (b) prediction of the fluctuation term displacement at point B (c) cumulative displacement prediction at point B (d) the cumulative displacement prediction interval at point B (see online version for colours)

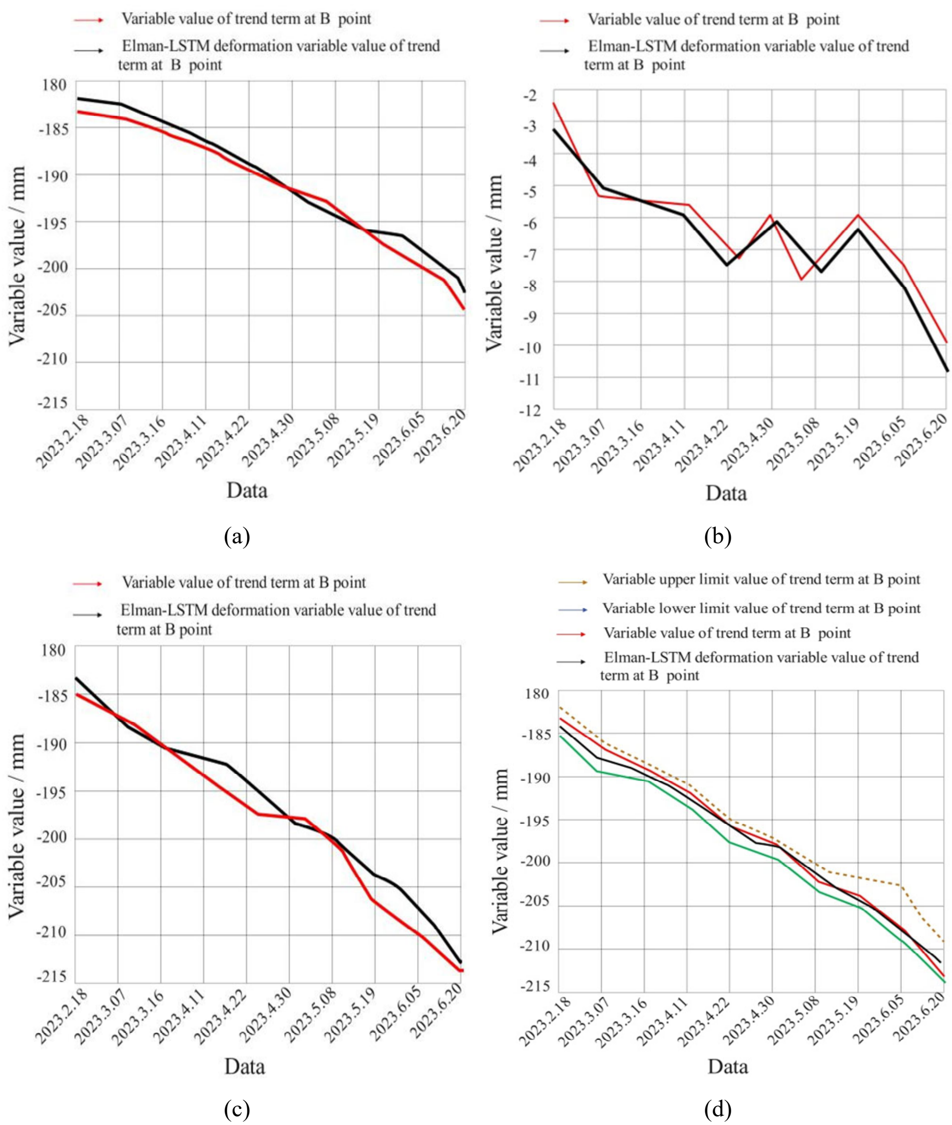

In order to analyse from the data aspect, the data in Figure 11 above are counted, and the corresponding absolute errors and relative errors are calculated. The specific values are shown in Table 2.

In order to evaluate the accuracy of the model, three indicators are selected: mean absolute error (MAE), root mean square error (RMSE), and R^2 certainty coefficient for model evaluation. The test results of the four models are compared together. The results are shown in Table 3 and Table 4.

In order to further verify the progressiveness of the model in this paper, the model in this paper is compared with Liu et al. (2021), Leber et al. (2020), Liu e al. (2020) and Kozyreva et al. (2022). Liu et al. (2021) use an in-depth learning model, Leber et al. (2020) use a multi-mode deformation monitoring model, Liu e al. (2020) use a wireless sensor network model, and Kozyreva et al. (2022) use a geomagnetic field disturbance model. Through simulation and comparison of prediction accuracy, a total of four groups of tests were carried out, and the comparison results of displacement prediction accuracy shown in Table 5 were obtained.

Table 1 Displacement prediction accuracy and error comparison (A) of Elman-LSTN

Date	*True value/mm*	*Predicted value/mm*	*Absolute error*	*Relative error (%)*
2023.2.18	86.4468	86.7933	0.3465	0.40%
2023.3.07	85.1202	85.4073	0.2871	0.34%
2023.3.16	86.2884	86.6151	0.3267	0.38%
2023.4.11	86.5953	86.9220	0.3267	0.37%
2023.4.22	88.7139	88.9416	0.2277	0.26%
2023.4.30	92.1591	92.1987	0.0396	0.04%
2023.5.08	90.9513	90.6642	0.2871	0.32%
2023.5.19	92.3373	91.9611	0.3762	0.41%
2023.6.05	94.0797	93.5550	0.5247	0.55%
2023.6.20	96.4359	95.6835	0.7524	0.77%

Table 2 Displacement prediction accuracy and error comparison (B) of Elman-LSTN

Date	*True value/mm*	*Predicted value/mm*	*Absolute error*	*Relative error (%)*
2023.2.18	181.665	182.3679	0.7029	0.39%
2023.3.07	185.229	186.0507	0.8217	0.44%
2023.3.16	187.506	188.2683	0.7623	0.40%
2023.4.11	189.981	190.5354	0.5544	0.29%
2023.4.22	193.842	194.1588	0.3168	0.16%
2023.4.30	195.624	195.9705	0.3465	0.18%
2023.5.08	199.485	199.7424	0.2574	0.13%
2023.5.19	201.267	201.2274	0.0396	0.02%
2023.6.05	204.831	204.5934	0.2376	0.12%
2023.6.20	209.979	210.1077	0.1287	0.06%

Table 3 Precision evaluation of four displacement prediction models (point A)

	Cumulative displacement			*Trend term*			*Fluctuation term*		
	MAE	*RMSE*	*R^2*	*MAE*	*RMSE*	*R^2*	*MAE*	*RMSE*	*R^2*
SVM	1.306	1.330	0.858	1.200	1.200	0.745	0.243	0.275	0.961
LSTM	0.866	1.143	0.892	0.860	1.183	0.752	0.082	0.113	0.985
Elman	0.558	0.603	0.963	0.364	0.446	0.956	0.267	0.340	0.946
Elman-LSTM	0.348	0.391	0.979	0.357	0.418	0.960	0.040	0.051	0.989

Table 4 Precision evaluation of four displacement prediction models (point B)

	Cumulative displacement			*Trend term*			*Fluctuation term*		
	MAE	*RMSE*	R^2	*MAE*	*RMSE*	R^2	*MAE*	*RMSE*	R^2
SVM	1.300	1.433	0.962	1.086	1.090	0.966	0.444	0.557	0.894
LSTM	0.970	1.097	0.974	1.004	1.216	0.960	0.289	0.333	0.955
Elman	0.717	0.896	0.979	0.572	0.679	0.981	0.524	0.644	0.861
Elman-LSTM	0.417	0.492	0.987	0.434	0.487	0.985	0.197	0.280	0.966

Table 5 Comparison of displacement prediction accuracy

	Yang et al. (2020)	*Leber et al. (2020)*	*Liu et al. (2020)*	*Kozyreva et al. (2022)*	*This article*
1	82.21	83.28	65.42	91.18	99.47
2	73.48	85.98	65.79	90.65	98.86
3	74.75	80.07	68.77	93.19	98.10
4	73.74	83.55	71.35	87.71	97.25

4.4 Analysis and discussion

It can be seen from Figure 10(a) that the trend term deformation prediction curve of N-point is basically consistent with the real deformation curve, but there is a small amount of error between February 18, 2023 and June 20, 2023. Figure 10(b) shows the change trend between the predicted value and the real value of the wave term displacement. It can be seen from the figure that the predicted value basically coincides with the real deformation value, and the predicted result is close to the real value. Figure 10(c) reflects the change trend between the cumulative deformation predicted value and the deformation value. It can be seen from the figure that the predicted value and the deformation value basically overlap, and the change trend is basically the same. However, after May 8, 2023, there are small fluctuations. The main reason is the result affected by the prediction of the trend term. Figure 10(d) shows a reliable change interval of the deformation value (± 1 mm), and it can be clearly seen that the predicted result of the cumulative displacement at N points is within the predicted interval and is basically close to the real value. To sum up, it can be seen that Elman-LSTM has the highest overall prediction accuracy for the trend term displacement, fluctuation term displacement, and cumulative displacement of point N, and the prediction curves of the three displacements are highly consistent with the real curve. Compared with the other three methods, the overall prediction effect is the best.

It can be seen from Table 1 that the maximum absolute error of point A is 0.752, the minimum is 0.036, and the average absolute error is 0.347. The maximum relative error is 0.772%, the minimum is 0.036%, and the average relative error is 0.376%. All predicted values are within the allowable range of error. To sum up, it can be seen that the cumulative displacement prediction of point A based on Elman-LSTM has the smallest deviation between the cumulative predicted value and the real value, and the prediction effect is the best.

It can be seen from Figure 11(a) that the deformation prediction curve of the trend term at point A is basically consistent with the real deformation curve. However, there are small-scale fluctuations before April 22, 2023 and after May 19, 2023, which may be related to the influence of external factors such as rainfall. Figure 11(b) shows the change trend between the predicted value of the fluctuation term and the real value. It can be seen from the figure that the predicted value of the displacement of the fluctuation term is basically consistent with the real deformation value. Among them, the predicted results from March 16, 2023 to April 30, 2023 are close to the real value, and the effect is the best. Figure 11(c) reflects the change trend between the cumulative deformation prediction value and the deformation value. It can be seen from the figure that the predicted value and the deformation value basically coincide, but there will be a small range of fluctuations before April 11, 2023. It is mainly affected by the predicted displacement of the trend item. Figure 11(d) shows a reliable variation interval of the deformation value (± 1 mm), and it can be clearly seen that the predicted result of the cumulative displacement at point A is within the predicted interval. To sum up, it can be seen that Elman-LSTM has the highest overall prediction accuracy for the trend term displacement, wave term displacement, and cumulative displacement of point A, and the prediction curves of the three displacements are highly consistent with the real curves, and the overall prediction effect is the best.

It can be seen from Table 2 that the maximum absolute error of point A is 0.82, the minimum is 0.0396, and the average absolute error is 0.4158. The maximum relative error is 0.436%, the minimum is 0.02%, and the average relative error is 0.218%. All predicted values are within the allowable range of error. To sum up, it can be seen that the cumulative displacement prediction of point A based on Elman-LSTM has the smallest deviation between the cumulative predicted value and the real value, and the prediction accuracy is the highest.

From Table 3, it can be seen that the accuracy of the Elman-LSTM joint model is higher than that of the other three prediction models. The Elman-LSTM joint model shows an obvious trend of accuracy improvement in the prediction of the two sampling points. The reason may be that subsidence displacement is a dynamic change process, while SVM belongs to a static prediction model. This model only learns and uses the information at the current time, and cannot use historical information. However, both LSTM and Elman belong to dynamic prediction models. When predicting the current displacement change value, it will first recall the displacement data of the previous period, and then predict the displacement value at the current time, so as to achieve dynamic prediction, so the prediction effect is better than SVM. In summary, the dynamic prediction model is more suitable for subsidence displacement monitoring.

Compared with the SVM model, the maximum difference of the average absolute error MAE of Elman-LSTM model is 1.382, the root mean square error RMSE is 1.364, and the certainty coefficient R^2 is 0.121. Compared with the LSTM model, the maximum difference of the average absolute error MAE of the cumulative displacement prediction of the Elman-LSTM model is 0.552, the maximum difference of the root mean square error RMSE is 0.753 and the maximum difference of the certainty coefficient R^2 0.086. Compared with the Elman model, the maximum difference of the average absolute error MAE of the cumulative displacement prediction of the Elman-LSTM model is 0.299, the maximum difference of the root mean square error RMSE is 0.404, and the maximum difference of the certainty coefficient R^2 is 0.0158.

From the results in Table 5, it can be seen that the model proposed in this paper has a very high prediction accuracy and has significant advantages compared to existing research.

On the whole, the model of monitoring and early warning of regional subsidence of transmission lines based on time series algorithm proposed in this paper has certain effect, and can meet the needs of monitoring and early warning of regional subsidence of transmission lines.

5 Conclusions

The ground subsidence of high-voltage line tower area has become a serious problem affecting the stability and security of transmission lines. Therefore, it is very important to monitor and warn the regional subsidence of high-voltage towers. Based on the satellite-borne InSAR technology, this paper studies the relevant theories and technologies of monitoring and early warning of regional subsidence of high-voltage towers, and proposes a method for early warning and evaluation of regional subsidence of high-voltage towers. Moreover, this paper uses autoformer-based regional subsidence prediction model of high-voltage line towers to predict the subsidence value of monitoring points in the study area, and calculate the surface subsidence rate. In addition, according to the cumulative subsidence value and subsidence rate, a complete regional subsidence early warning model for high-voltage line towers is established in this paper. In general, the model of monitoring and early warning of regional subsidence of transmission lines based on time series algorithm proposed in this paper has certain effect, and can meet the needs of monitoring and early warning of regional subsidence of transmission lines.

In the InSAR time-series meteorological and environmental subsidence dataset constructed in this article, only the influence of meteorological and environmental factors on surface subsidence was considered, without taking into account the impact of human activities, engineering plans, and other human factors on surface subsidence in the high-voltage transmission tower area. Moreover, the data in this article was not validated through large-scale practical experiments. Therefore, in future work, the above factors will be considered as features and included in the dataset for model training and testing, establishing a more comprehensive dataset to obtain more accurate prediction results of cumulative subsidence values in the high-voltage transmission tower area.

Acknowledgements

Supported by the Science and Technology Project of State Grid Sichuan Electric Power Company, the fund project name is Research on Communication, Protection, and Stability Control Coupling Simulation Analysis Technology Based on Regulation Cloud (521911230001)

References

Abasi, M., Heydarzadeh, N. and Rohani, A. (2022) 'Broken conductor fault location in power transmission lines using GMDH function and single-terminal data independent of line parameters', *Journal of Applied Research in Electrical Engineering*, Vol. 1, No. 1, pp.22–32.

Ansari, S., Ayob, A., Lipu, M.S.H., Saad, M.H.M. and Hussain, A. (2021) 'A review of monitoring technologies for solar PV systems using data processing modules and transmission protocols: progress, challenges and prospects', *Sustainability*, Vol. 13, No. 15, pp.8120–8131.

Brito Palma, L. (2024) 'Hybrid approach for detection and diagnosis of short-circuit faults in power transmission lines', *Energies*, Vol. 17, No. 9, pp.2169–2180.

Chehri, A., Jeon, G., Fofana, I., Imran, A. and Saadane, R. (2021) 'Accelerating power grid monitoring with flying robots and artificial intelligence', *IEEE Communications Standards Magazine*, Vol. 5, No. 4, pp.48–54.

Chen, C., Yuan, G., Zhou, H. and Ma, Y. (2023) 'Improved YOLOv5s model for key components detection of power transmission lines', *Mathematical Biosciences and Engineering*, Vol. 20, No. 5, pp.7738–7761.

Chen, C., Zhang, Y., Zhao, H., Peng, Z. and Wang, Q. (2024) 'Acoustic carrier signal transmission technology and its potential for in-site monitoring of sliding electrical contact used in gas-insulated switchgear/gas-insulated transmission line', *High Voltage*, Vol. 9, No. 2, pp.287–295.

Chen, W. (2020) 'Intelligent manufacturing production line data monitoring system for industrial internet of things', *Computer Communications*, Vol. 151, No. 1, pp.31–41.

Godse, R. and Bhat, S. (2020) 'Mathematical morphology-based feature-extraction technique for detection and classification of faults on power transmission line', *IEEE Access*, Vol. 8, No. 1, pp.38459–38471.

Huang, X. (2020) 'Intelligent remote monitoring and manufacturing system of production line based on industrial internet of things', *Computer Communications*, Vol. 150, No. 1, pp.421–428.

Khayrullaev, A. (2023) 'UDC: 004.4; 621.315. 1 Microcontroller-based remote monitoring of overhead power lines', *Scientific and Technical Journal of Namangan Institute of Engineering and Technology*, Vol. 8, No. 2, pp.228–236.

Kozyreva, O.V., Pilipenko, V.A., Marshalko, E.E., Sokolova, E.Y. and Dobrovolsky, M.N. (2022) 'Monitoring of geomagnetic and telluric field disturbances in the Russian Arctic', *Applied Sciences*, Vol. 12, No. 8, pp.3755–3766.

Lazzaretti, A.E., Costa, C.H.D., Rodrigues, M.P., Yamada, G.D., Lexinoski, G., Moritz, G.L. and Santos, R.B.D. (2020) 'A monitoring system for online fault detection and classification in photovoltaic plants', *Sensors*, Vol. 20, No. 17, pp.4688–4700.

Leber, A., Dong, C., Chandran, R., Das Gupta, T., Bartolomei, N. and Sorin, F. (2020) 'Soft and stretchable liquid metal transmission lines as distributed probes of multimodal deformations', *Nature Electronics*, Vol. 3, No. 6, pp.316–326.

Li, Q., Zhang, L., Zhang, C., Tian, Y., Fan, Y., Li, B. and Wang, Z.L. (2024) 'Compact, robust, and regulated-output hybrid generators for magnetic energy harvesting and self-powered sensing applications in power transmission lines', *Energy & Environmental Science*, Vol. 17, No. 8, pp.2787–2799.

Liu, C., Wu, Y., Liu, J., Sun, Z. and Xu, H. (2021) 'Insulator faults detection in aerial images from high-voltage transmission lines based on deep learning model', *Applied Sciences*, Vol. 11, No. 10, pp.4647–4660.

Liu, J., Zhao, Z., Ji, J. and Hu, M. (2020) 'Research and application of wireless sensor network technology in power transmission and distribution system', *Intelligent and Converged Networks*, Vol. 1, No. 2, pp.199–220.

Rodríguez-Arana, B., Ciáurriz, P., Gil-Negrete, N. and Alvarado, U. (2023) 'A non-intrusive monitoring system on train pantographs for the maintenance of overhead contact lines', *Sensors*, Vol. 23, No. 18, pp.7890–7899.

Wu, H., Wang, J., Wu, Z., Kang, S., Wei, X., Wang, H. and Wang, Z.L. (2022) 'Multi-parameter optimized triboelectric nanogenerator based self-powered sensor network for broadband aeolian vibration online-monitoring of transmission lines', *Advanced Energy Materials*, Vol. 12, No. 13, pp.2103654–2103665.

Wu, K.E., Bozzi, M. and Fonseca, N.J. (2021) 'Substrate integrated transmission lines: review and applications', *IEEE Journal of Microwaves*, Vol. 1, No. 1, pp.345–363.

Xu, C., Li, Q., Zhou, Q., Zhang, S., Yu, D. and Ma, Y. (2022) 'Power line-guided automatic electric transmission line inspection system', *IEEE Transactions on Instrumentation and Measurement*, Vol. 71, No. 1, pp.1–18.

Yang, L., Fan, J., Liu, Y., Li, E., Peng, J. and Liang, Z. (2020) 'A review on state-of-the-art power line inspection techniques', *IEEE Transactions on Instrumentation and Measurement*, Vol. 69, No. 12, pp.9350–9365.